DOI: 10.1021/ma901219a

Macromolecules
ARTICLE

Half-Metallocene Titanium(IV) Phenyl Phenoxide for High Temperature Olefin Polymerization: Ortho-Substituent Effect at Ancillary *o*-Phenoxy Ligand for Enhanced Catalytic Performance

Tae-Jin Kim,[†] Sung-Kwan Kim,[†] Beom-Jun Kim,[†] Jong Sok Hahn,[‡] Myung-Ahn Ok,[‡] Jong Hee Song,[‡] Dae-Ho Shin,[‡] Jaejung Ko,[†] Minserk Cheong,[§] Jin Kim,[⊥] Hoshik Won,[⊥] Mariusz Mitoraj,[∥] Monika Srebro,[∥] Artur Michalak,*[,∥] and Sang Ook Kang*[,†]

[†]*Department of Advanced Material Chemistry, Korea University, Sejong, Chungnam 339-700, South Korea,* [‡]*SK Energy R&D Center, 140-1 Wonchon-dong, Yuseong-gu, Daejeon 305-712, Korea,* [§]*Department of Chemistry and Research Institute for Basic Sciences, Kyung Hee University, Seoul 130-701, Korea,* [⊥]*Department of Chemistry & Applied Chemistry, Hanyang University, Ansan 425-791, Korea, and* [∥]*Department of Theoretical Chemistry, Faculty of Chemistry, Jagiellonian University, R. Ingardena 3, 30-060 Kraków, Poland*

Received June 8, 2009; Revised Manuscript Received July 28, 2009

ABSTRACT: A series of mono- or dialkyl/phenyl *o*-substituted phenoxy ligands in half-metallocene titanium(IV) complexes was examined to determine the structure-catalytic activity relationship in high temperature olefin polymerization. Five different types of polymerization catalysts with different Cp/Cp* and mono- or disubstituted symmetric/asymmetric alkyl/phenyl phenoxide ancillary ligands were compared. This series was examined for ethylene homopolymerization after activation with $Ph_3CB(C_6F_5)_4$ and mMAO-7 at high temperatures (140 °C). Type 4 complexes of compounds **15**−**18** [33.0−39.0 kg/(mmol of Ti·h)] showed much higher catalytic activity than those found in types 1−3 and 5 [3.6−27.6 kg/(mmol of Ti·h)], and among the type 4 complexes, the Cp*/2-phenylphenoxy combination of compound **18** [39 kg/(mmol of Ti·h)] surpassed the Cp*/2-alkyl ligand systems of compounds **15**−**17** [33.0−36.0 kg/(mmol of Ti·h)]. The revolving nature of the phenoxy ligand around the Ti−O−C axis was identified by the NOSEY correlation peaks between the methyl protons of Cp* and protons of ancillary phenyl phenoxy ligand in compound **18**. The conformational flexibility of the phenyl phenoxy ligand was further confirmed by a series of temperature-dependent ROSEY experiments based on the optimization of two conformational structures related by this rotation. Rotational barriers of 4.3 and 6.6 kcal/mol were estimated from theoretical DFT studies. DFT calculations of the transition states for ethylene insertion and termination were carried out for representative examples of types 4 (**15**, **16**, **18**), 3 (**10**, **12**), and 1 (**3**) catalysts as well as the constrained geometry catalyst (CGC) as a reference. The preference for back-side insertion was a unique feature of the monosubstituted type 4 catalysts. The type 4 catalysts showed significant activities for ethylene/1-octene copolymerization affording high molecular weight poly(ethylene−*co*−1−octene)s (M_w = 107 000 −164 000) with unimodal molecular weight distributions (M_w/M_n = 2.08−4.15). The activity increased in the order of type 3 [90−132 kg/(mmol of Ti·h), in toluene, ethylene 30 atm, 1-octene 8 mL, 140 °C, 10 min.] < CGC (222) < type 4 (228−354). Among the type 4 series, compound **18** showed the best performance, reaching an activity of 354 kg/(mmol of Ti·h). The polymer density of 0.9148 g/mL for compound **18** was lower than that found in CGC (0.9154 g/mL), indicating higher 1-octene incorporation, which was further confirmed by an analysis of the ^{13}C NMR spectra of the polymers (**18**, 2.73 mol % and CGC, 2.55 mol %).

Introduction

High temperature olefin polymerization using a single site catalyst remains a challenge in the polyolefin industry. There has been increasing interest in the development of new, postmetallocene single site catalysts[1] due to the growing demand for special grade polyolefins, such as LLDPE (linear low density polyethylene),[2] VLDPE (very low density polyethylene),[3] and polyolefin elastomers.[4] Particular attention has been paid to half-metallocenes[5] because they can be used to introduce a variety of ancillary ligands without synthetic difficulty. Thus far, CGC-type complexes, such as Dow Constraint[6] and Sumitomo Phenics catalytic systems,[7] are highly active catalytic systems. In recent years, Stephan reported phosphinimine-based catalysts with remarkable catalytic activity at high temperatures.[8] Such a high catalytic activity was attributed to the ligand consisting of a sterically bulky substituent on the phosphorus atom and the effective protection around the metal center. Phenoxy titanium half-sandwich complexes, where the 2,6-position of the phenoxy ligand was substituted with either by alkyl or phenyl groups, were studied extensively by Nomura[9] and Rothwell,[10] respectively. In particular, enhanced catalytic performance on olefin polymerization was observed when the 2,6-position at the phenoxy ligand was substituted with bulky groups, such as isopropyl or *tert*-butyl, and this was examined thoroughly by Nomura.[9]

As part of an ongoing study into the development of new catalytic systems for applications in high temperature solution processes, the modification of half-metallocene titanium(IV) complexes was one of the intended research areas, where the catalytic performance can be improved easily by altering the ancillary ligand structure. On the basis of cyclopentadienide

*Corresponding authors. (S.O.K.) E-mail: sangok@korea.ac.kr. Fax: +82-41-867-5396. (A.M.) E-mail: michalak@chemia.uj.edu.pl. Fax: +48-12-634-0515.

 Published on Web 08/21/2009

Chart 1. Five Different Types of Piano-Stool Half-Titanocenes with the Variation 2,6-Di- and 2-Mono-Substituted Phenoxide Ligands

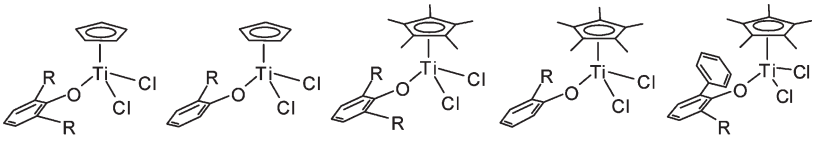

Type 1	Type 2	Type 3	Type 4	Type 5
R = H **1**	R = Me **6**	R = H **10**	R = Me **15**	R = Me **19**
Me **2**	*i*-Pr **7**	Me **11**	*i*-Pr **16**	*i*-Pr **20**
i-Pr **3**	*t*-Bu **8**	*i*-Pr **12**	*t*-Bu **17**	*t*-Bu **21**
t-Bu **4**	Ph **9**	*t*-Bu **13**	Ph **18**	
Ph **5**		Ph **14**		

Cp/Cp* and 2,6-di-/2-monosubstitued phenoxy ligand combinations, five different ensembles (herein referred to as types 1−5) were proposed and tested for high temperature olefin polymerization at 140 °C. Type 4 complexes of compounds **15**−**18** with 2-monosubstituted phenoxide and a Cp* combination exhibited much higher catalytic activity [33.0−39.0 kg/(mmol of Ti·h)] than those found in types 1−3 and 5 [3.6−27.6 kg/(mmol of Ti·h)]. Among the type 4 complexes, the Cp*/2-phenylphenoxy combination of compound **18** [39 kg/(mmol of Ti·h)] surpassed the Cp*/2-alkyl ligand systems of compounds **15**−**17** [33.0−36.0 kg/(mmol of Ti·h)]. In particular, the 2-phenylphenoxy ligand system exhibited enhanced conformational flexibility due to the presence of an *o*-phenyl substituent, which was suggested by both the DFT calculations and observed by NMR. Furthermore, the DFT calculation suggested that a back-side insertion mechanism was the origin of such high catalytic activity. The phenylphenoxy system **18** showed the highest catalytic activity of 354 kg/(mmol of Ti·h) for ethylene/1-octene copolymerization, affording a high molecular weight poly(ethylene−*co*−1−octene)s (M_w = 164 000) with a unimodal molecular weight distribution (M_w/M_n = 3.01) and higher 1-octene incorporation of 2.73 mol %.

Results and Discussion

Synthesis and Characterization of Type 1−5. Compounds **1**−**14** were obtained using the procedures reported elsewhere.[5c,9a,11] A Pd-catalyzed Suzuki-type cross-coupling reaction between the 2-alkyl-6-bromoanisole (R = Me, *i*-Pr, and *t*-Bu) and phenylboronic acid was carried out to yield the 2-alkyl-6-phenylanisole in high yield (90−95%). The desired 2-alkyl-6-phenylphenols were produced using a deprotection procedure (95−97%). (Scheme 1) The 2-alkyl/phenyl and 2-alkyl-6-phenylphenoxy coordinated titanium half-metallocenes of the type Cp*Ti(O-2-R_1-6-R_2Ph)Cl_2 (R_1 = Me, R_2 = H (**15**); R_1 = *i*-Pr, R_2 = H (**16**); R_1 = *t*-Bu, R_2 = H (**17**); R_1 = Ph, R_2 = H (**18**); R_1 = Me, R_2 = Ph (**19**); R_1 = *i*-Pr, R_2 = Ph (**20**); R_1 = *t*-Bu, R_2 = Ph (**21**)) were prepared by a reaction between Cp*$TiCl_3$ and 1 equiv of the Li-salt of 2-alkyl/phenyl- and 2-alkyl-6-phenylphenol at room temperature for 12 h. Recrystallization from a concentrated toluene solution at −15 °C produced compounds **15**−**21** as red crystals (75−85%). (Chart 1) The phenoxide coordination to the titanium center was confirmed by the ^{1}H NMR spectra of compounds **15**−**18**. Furthermore, methyl resonance on the Cp* of each titanium phenoxide was indicative of the presence of secondary interactions between the methyl groups of the Cp* and phenyl substituent at the 2-position of the phenoxy ligands. In the ^{1}H NMR spectra of compounds **15**−**17**, the methyl protons of Cp* resonate at a significantly lower field, δ 1.85−1.98 ppm, than the δ 1.67 observed for compound **18** (see Experimental Section). This suggests an enhanced interaction caused by the phenyl substituent at the 2-position of the phenolate ligand.

Scheme 1. Preparation of 2-Alkyl-6-phenylphenol

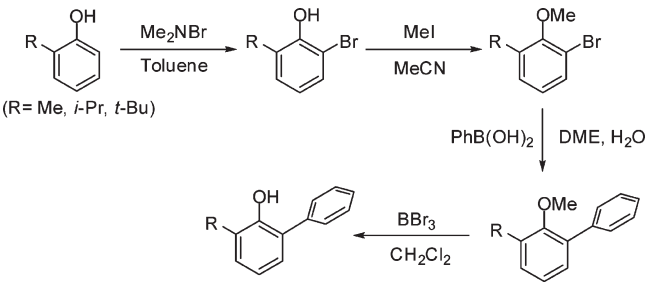

Considerable interactions arose due to the proximity of the phenyl ring to the methyl group of the Cp* unit.[12]

Crystal Structures of Compounds 16, 18, and 21. Deep-red block microcrystals were grown from a concentrated toluene solution after standing at −15 °C. The influence of phenoxy ligands was examined by determining the crystal structures of compounds **16**, **18**, and **21** by X-ray crystallography using Bruker SMART CCD detector system (Mo Kα radiation, λ = 0.71073 Å). (Table 1) Figures 1−3 show the ORTEP drawings for compounds **16**, **18**, and **21**. The X-ray structures of compounds **16** (Figure 1) and **18** (Figure 2) showed a pseudotetrahedral geometry. The Ti−O bond lengths [**16**, 1.772(2) Å; **18**, 1.784(2) Å] were similar to those found in the disubstituted complexes **12**[9a] and **14**[11a] [1.772(2) and 1.811(3) Å, respectively] and the less bulky cyclopentadienyl complex **9**[13] [1.782(1) Å]. The Ti−Cl bond lengths in compound **18** [2.260(1) and 2.268(1) Å] were the same as those found in compound **9** [2.2572(6) and 2.2631(6) Å] and were somewhat shorter than those found in compound **14** [2.269(1) and 2.287(1) Å]. In addition, the O−C(11) bond lengths in compounds **16** and **18** [1.350(4) and 1.366(4) Å] were similar to the other phenoxide complexes found in compounds **9**, **12**, and **14** [1.366(2)−1.369(5) Å]. Therefore, based on the bond length data, there appears to be little electronic or steric effect in this type of complex. In the monophenoxide complex of $TiCl_3$[O-2,6-^{t}Bu-4-Me-Ph], where the phenoxide ligand is the dominant π-donor and has no competition from a π-donor Cp ligand, the Ti−O bond length has a shorter value of 1.750(2) Å showing stronger phenoxide π-donation than would be expected for the Cp-phenoxide complexes.[14] The Ti−O−C(11) bond angle in compound **16** [166.7(2)°] was significantly smaller than those found in compound **12** [173.0°] due to the less steric bulkiness of the monosubstituted phenoxy ligand.

The X-ray crystal structure determination of compound **21** (Figure 3) showed a pseudotetrahedral geometry similar to those found in the 2-monosubstituted systems of compounds **16** and **18**. The Ti−O bond length [1.813(1) Å] was longer and the Cl(1)−Ti−Cl(2) bond angle in compound **21** [97.69(3)°] was significantly smaller than those found in

Table 1. Crystal Data and Structure Refinement for Compounds 16, 18, and 21

	16	18	21
empirical formula	$C_{19}H_{26}Cl_2OTi$	$C_{22}H_{24}Cl_2OTi$	$C_{26}H_{32}Cl_2OTi$
formula weight	389.20	423.21	479.32
temperature	293(2) K	233(2) K	293(2) K
wavelength	0.71073 Å	0.71073 Å	0.71073 Å
crystal system, space group	orthorhombic, $P2_12_12_1$	orthorhombic, $Pna2_1$	monoclinic, $P2_1/c$
unit cell dimensions	a = 8.737(3) Å, α = 90°	a = 17.4895(10) Å, α = 90°	a = 7.9235(8) Å, α = 90°
	b = 13.852(5) Å, β = 90°	b = 7.4379(4) Å, β = 90°	b = 8.6579(9) Å, β = 93.438(2)°
	c = 16.094(5) Å, γ = 90°	c = 16.0058(9) Å, γ = 90°	c = 36.021(4) Å, γ = 90°
volume	1947.9(12) Å^3	2082.1(2) Å^3	2466.6(4) Å^3
Z, calculated density	4, 1.327 Mg/m^3	4, 1.350 Mg/m^3	4, 1.291 Mg/m^3
μ	0.715 mm^{-1}	0.676 mm^{-1}	0.579 mm^{-1}
F(000)	816	880	1008
crystal size	0.41 × 0.19 × 0.08 mm	0.23 × 0.19 × 0.11 mm	0.37 × 0.26 × 0.18 mm
θ range for data collection	1.94 to 28.37°	2.33 to 28.31°	2.27 to 28.32°
limiting indices	$-11 \le h \le 7$, $-18 \le k \le 18$, $-21 \le l \le 18$	$-23 \le h \le 23$, $-9 \le k \le 9$, $-21 \le l \le 21$	$-10 \le h \le 10$, $-11 \le k \le 11$, $-47 \le l \le 48$
no. of reflections collected/unique	14390/4878 [R_{int} = 0.0496]	20408/5142 [R_{int} = 0.0577]	32575/6162 [R_{int} = 0.0296]
max. and min transmission	0.9476 and 0.7556	0.9294 and 0.8601	0.9020 and 0.8166
Completeness to θ = 28.43	99.9%	99.9%	99.9%
refinement method	full-matrix least-squares on F^2	full-matrix least-squares on F^2	full-matrix least-squares on F^2
data/restraints/parameters	4878/0/215	5142/1/235	6162/0/279
goodness-of-fit on F^2	1.002	1.015	1.070
final R indices [$I > 2\sigma(I)$]	R_1 = 0.0437, wR_2 = 0.0935	R_1 = 0.0431, wR_2 = 0.0874	R_1 = 0.0564, wR_2 = 0.1499
R indices (all data)	R_1 = 0.1038, wR_2 = 0.1159	R_1 = 0.0945, wR_2 = 0.1095	R_1 = 0.0726, wR_2 = 0.1628
largest diff. peak and hole	0.330 and −0.189 e·Å^{-3}	0.374 and −0.257 e·Å^{-3}	0.547 and −0.352 e·Å^{-3}

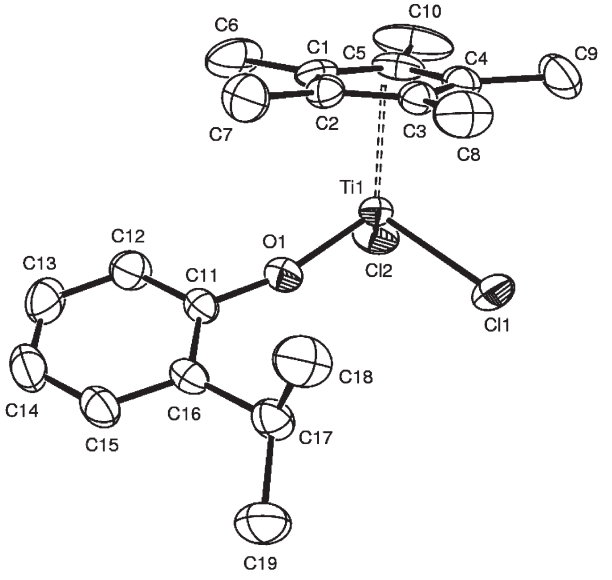

Figure 1. Molecular structures of compound **16** with thermal ellipsoids drawn at the 30% level.

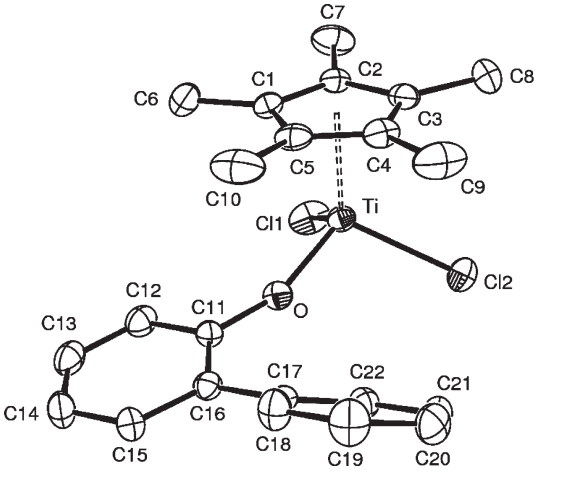

Figure 2. Molecular structures of compound **18** with thermal ellipsoids drawn at the 30% level.

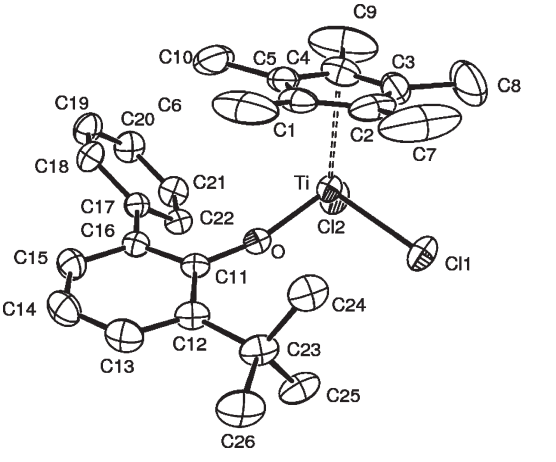

Figure 3. Molecular structures of compound **21** with thermal ellipsoids drawn at the 30% level.

compounds **16** and **18** [102.52(5) and 103.13(5)°, respectively]. This difference was attributed to the steric influence of the phenoxy group containing disubstituent groups in the 2,6-position. The C(11)−O bond length in compound **21** [1.369(3) Å] was similar to that of the other phenoxide complexes **16** and **18**.

Variable Temperature ^{1}H NMR Spectra and Nuclear Overhauser Effect (NOESY). The ^{1}H NMR spectrum of compound **18** at low temperatures (down to −70 °C) was similar to that obtained at room temperature, showing only one set of 12 phenyl phenoxy protons resonances and one set of methyl peaks for Cp* (see Figure 4). Such temperature-independent behavior indicated either that the 2-phenylphenoxy ligand is rotating rapidly on the NMR time scale at all temperatures, or that it is not rotating at all. A. J. Nielson et al.[13] reported the results of their preparative and structural studies of titanium complexes containing 2-alkylphenoxy ligands. On the basis of the DFT calculations, the existence of a shallow minimum associated with the Ti−O−C−C

dihedral angle was suggested. Therefore, the sufficient flexibility of the phenoxy ligand allowed torsional motion to accommodate the *tert*-butyl group in the observed position. Compound **18** has an untethered 2-phenylphenoxy ligand, which is similar to the above 2-*tert*-butylphenoxy ligand. Therefore it is reasonable to assume that at low temperatures, the 2-phenylphenoxy ligand of compound **18** rotates relatively rapidly. Because the ^{1}H NMR spectrum of compound **18** does not change significantly upon cooling, it can be concluded that the 2-phenylphenoxy ligand is rotating rapidly on the NMR time scale. The rapid rotation of the 2-phenylphenoxy ligands at room temperatures was confirmed by the NOESY spectra (Figure 5), in which cross peaks of the methyl of Cp* protons with both the "b" and "c" protons of the *ortho*-phenyl substituent are present. In addition, the cross-peak of methyl of Cp* protons with the "g" proton of the phenoxy ligand was observed, as expected for a rotating 2-phenylphenoxy ligand.[14]

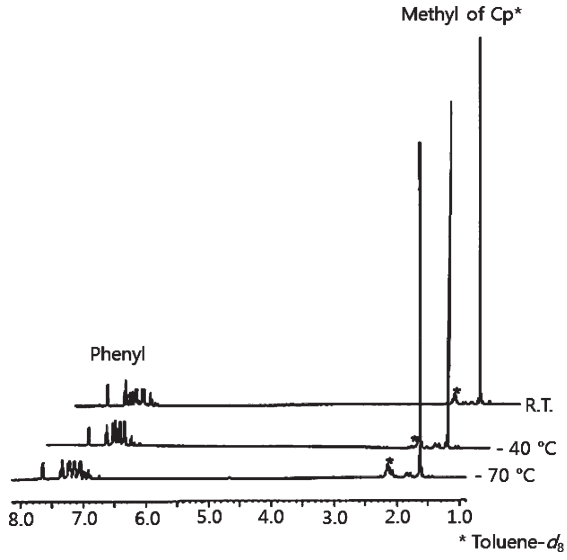

Figure 4. Variable-temperature ^{1}H NMR spectra of compound **18**, in toluene-d_8 from −70 °C to room temperature.

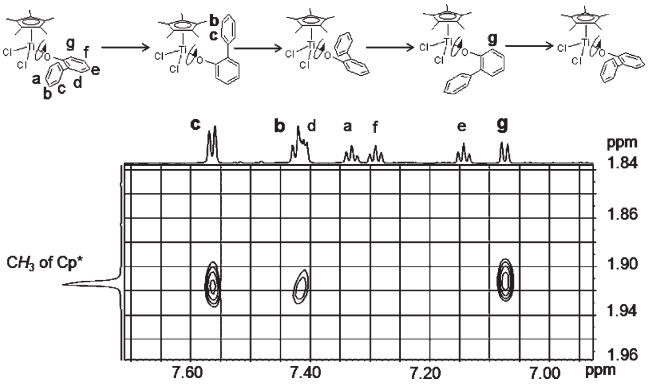

Figure 5. 800 MHz ^{1}H-NOESY spectrum of compound **18**, demonstrating a revolution of the phenylphenoxy ligand along the Ti−O−C(11) axis evidenced by the strong nuclear Overhauser effects between methyl protons of Cp* and b, c, and g protons of the phenylphenoxy ligand.

Back-Calculation of Energetically Possible Two Conformers Based on Temperature-Dependent ROSEY Experiments. Two-dimensional ROESY back-calculations were carried out to determine the final distance geometry (DG) structures (Figure 6).[15] The algorithm (BKCALC) employs what is basically an empirical two-parameter fitting of the spectral density, one parameter ($k_{cr} = 75$ s^{-1}; determined by fitting the NOE buildup of geminal protons) governing the cross relaxation rate, and the other ($k_{zl} = 1$ s^{-1}, except for methyl protons, where $k_{zl} = 3$ s^{-1} was used; determined by measuring the loss of the integrated, total spectral magnetization as a function of the mixing time) controlling the "*z*-leakage" rate. *z*-Leakage accounts for the loss of *z*-magnetization due to all processes other than cross relaxation (e.g., multiple quantum, chemical exchange, etc.). This approach accurately accounts for spin diffusion.

Two-dimensional nuclear magnetic resonance (2D ROESY) spectroscopic methods were used in combination with the distance geometry and the Overhauser effect back-calculation computational methods to determine the solution-state structure of compound **18**. The NMR signal assignments were made for all nonexchangeable protons using double quantum filtered correlated (COSY), nuclear Overhauser effect (NOESY), and rotating frame Overhauser effect (ROESY) ^{1}H−^{1}H correlated spectroscopy. The three-dimensional structure of compound **18** was determined based on an approach developed originally to examine the biopolymers, which includes a back-calculation of the 2D ROESY spectra for the model structures generated by DG/SA computations. As a first step, the primary restraints that allowed for the maximum conformational flexibility in the absence of the ROE-derived distance information were derived. The structures generated with "loose" ROE-derived distance restraints [2.0−2.5, 2.0−3.5, and 2.0−4.5 Å for

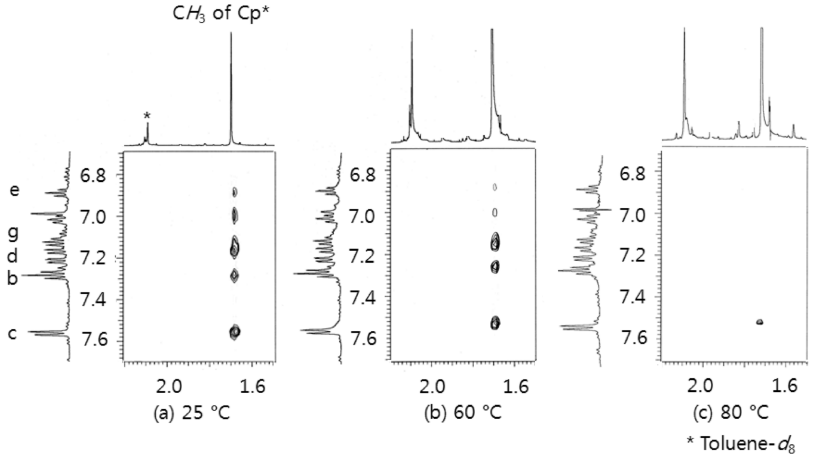

Figure 6. ^{1}H-ROESY spectrum of compound **18** (in toluene-d_8): (a) 25 °C; (b) 60 °C; (c) 80 °C.

Table 2. Cross Peaks[a] of ROESY of Compound 18

	25 °C (298.2 K)	60 °C (331.2 K)	80 °C (353.2 K)
Cp*	g (m), f (m′), e (w′), c (m), b(m′)	g (m), f (w′), e (w′), c (m), b (m′)	c (w′)
a	b (s)	b (s)	b (s)
b	Cp* (m′), c (s), a (s)	Cp* (m′), c (s), a (s)	c (s), a (s)
c	Cp* (m), d (s′), b (s)	Cp* (m), b (s)	Cp* (w′), b (s)
d	e (s), c (s′)	e (s)	e (s)
e	Cp* (w′), f (s), d (s)	Cp* (w′), f (s), d (s)	f (s), d (s)
f	Cp* (m′), g (s), e (s)	Cp* (w′), g (s), e (s)	g (s), e (s)
g	Cp* (m), f (s)	Cp* (m), f (s)	f (s)

[a] Intensity: s > s′ > m > m′ > w > w′.

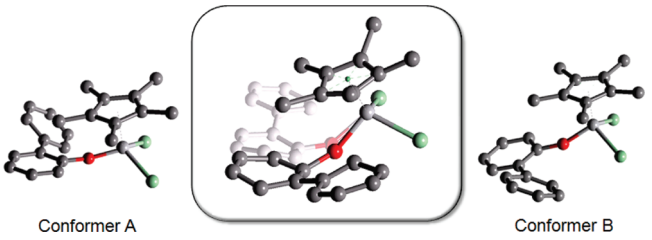

Figure 7. Two conformational isomer structures, related by revolving phenylphenoxy ligand optimized by a series of temperature-dependent ROSEY experiments.

Chart 2. Screening Catalysts for Ethylene Homopolymerization at 140 °C[a]

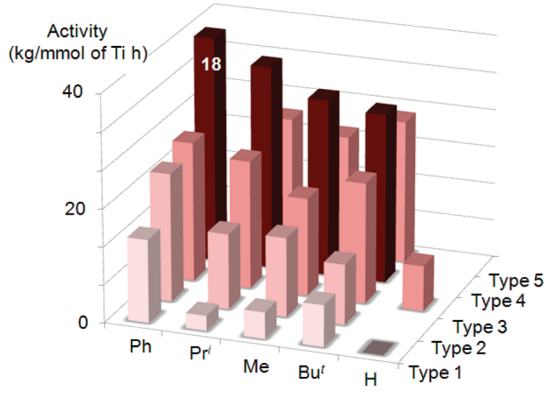

[a] Five different types of half-metallocene titanium(IV) complexes with the variation of ancillary ligands, Cp/Cp*, and mono- or disubstituted phenoxide.

strong (s and s′), medium (m and m′) and weak (w and w′) ROE cross peak intensities, respectively] converged to a unique conformation (Table 2), with pairwise root-mean-square deviation (rmsd) values for atoms in the range 2.0−4.5 Å. With the exception of some side-chain atoms, the back-calculated ROESY spectra of the DG/SA structures were consistent with the experimental ROESY spectrum. Two conformational isomer structures, which were related by the revolving phenylphenoxy ligand, were optimized by a series of temperature-dependent ROSEY experiments. (Figure 7)

Ethylene Homopolymerization. The newly prepared complexes were tested for ethylene homopolymerization after activation with $Ph_3CB(C_6F_5)_4$ and mMAO-7 at high temperatures (140 °C). The mMAO-7 was added as both an alkylating reagent and a scavenger of polar impurities. The results are shown in Chart 2. Table 3 summarizes the polymerization conditions and selected ethylene homopolymerization results. Compounds **15**−**18** [Type 4, 33.0−39.0 kg/(mmol of Ti·h)] exhibited much higher catalytic activity than those found in types 1−3 (**1**−**14**) and 5 (**19**−**21**) [3.6−27.6 kg/(mmol of Ti·h)] (see Supporting Information). Type

Table 3. Selected Results of Ethylene Homopolymerization[a]

type	catalyst	temp (°C)	yield (g)	activity[b]	M_w (×10^4)[c]	M_w/M_n[c]
3	**10**	140	4.2	25.2	35.1	3.12
	11	140	3.7	22.2	39.9	2.18
	12	140	4.6	27.6	31.6	2.28
	13	140	4.3	25.8	34.3	1.99
	14	140	3.5	21.0	31.7	2.38
4	**15**	140	5.7	34.2	30.6	2.68
	16	140	6.0	36.0	36.1	3.13
	17	140	5.5	33.0	27.7	2.47
	18	140	6.5	39.0	27.5	2.27
ref	CGC[d]	140	5.5	33.0	28.2	2.94

[a] Polymerization condition: semibatch type 200 mL autoclave reactor, cocatalyst = $[Ph_3C][B(C_6F_5)_4]$, scavenger = mMAO-7, solvent = cyclohexane, ethylene pressure = 30 kg/cm^2, total solution volume = 110 mL, catalyst = 1 μmol, [catalyst]:[cocatalyst]:[scavenger] = 1: 1.5: 100, reaction time = 10 min.; [b] kg of polymer/(mmol of Ti·h).; [c] Weight average molecular weight (g/mol) and molecular weight distribution were measured by PL210 GPC at 135 °C.; [d] $[Me_2Si(\eta^5\text{-}Me_4Cp)(N^tBu)]TiCl_2$.

5 differs from type 3 by the placement of two dissimilar substituents at each of the 2,6-positions of the phenoxy ligand, creating an asymmetric ligand environment. The molecular weight distributions (MWD) were quite narrow (M_w/M_n = 1.99−3.13). The activity of compound **18** [39.0 kg/(mmol of Ti·h)] was higher than compounds **15**−**17** and CGC [**15**, 34.2 kg/(mmol of Ti·h); **16**, 36.0 kg/(mmol of Ti·h); **17**, 33.0 kg/(mmol of Ti·h); CGC, 33.0 kg/(mmol of Ti·h)]. However, the molecular weight of the polyethylene obtained with compound **18** (M_w = 275,000) was the smallest among this series. This might be due to the open nature of monophenoxide ligand, which is also related to the higher copolymerization activity with 1-octene of this ligand, e.g., 2-phenyl phenoxide. Steric protection at the ligand center prevents either chain transfer or β-hydride elimination during polymerization to give a higher molecular weight. Catalyst **16** gave rise to the highest molecular weight polymer but further elaboration of the **15**, **17**, and **18** ligand systems was not definite. The molecular weight distributions were approximately M_w/M_n = 2.27−3.13 for type 4 and CGC complexes. In particular, those of compounds **15**−**18** with mMAO-7 as an alkylating reagent and a scavenger were close to the MWD value of 2.0 which correspond to a typical homogeneous catalyst system with a single-site character. The highest activity with the largest exotherm was observed from complex **18**, and the activity decreases in the order of type 4 > CGC > type 3 and type 5 > type 1 and type 2. In the case of the **18**/$Ph_3CB(C_6F_5)_4$ system, the phenylphenoxide ligand resulted in such an impressive increase in high temperature catalytic performance, reaching a maximum value of 39.0 kg/(mmol of Ti·h), which is well above the activity of CGC. This suggests that the catalytic activity depends on the ligand structure with a single substituent at the 2-position on the phenoxy ligand producing the highest catalytic activity.

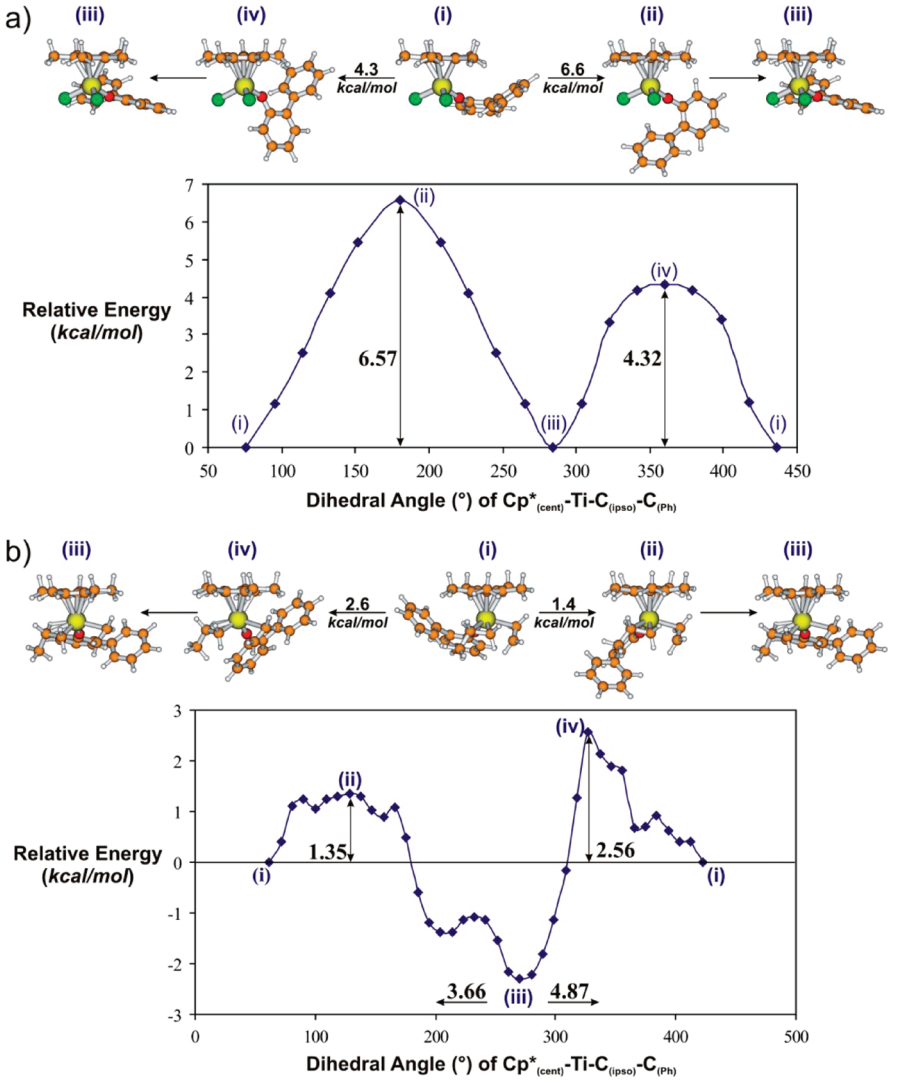

Figure 8. Energy profile for the rotation of the phenoxy ligand around the Ti−O−C(11) bonds for (a) the precatalyst **18** and (b) the corresponding ethylene π-complex.

Rotating 2-Phenylphenoxy Ligand and Back-Side Insertion Mechanism from DFT Calculations. The NOESY and ROESY study of compound **18** showed that a rotation of the phenoxide ligand is evident. A rotation of the 2-phenylphenoxy ligand around the Ti−O−C(11) bonds was examined theoretically using a DFT methodology for the precatalysts as well as for the active species (ethylene π-complexes). The results showed that such a rotation is feasible. Energy barriers of 4.3 and 1.4 kcal/mol were obtained for the precatalyst **18** and corresponding ethylene π-complex (Figure 8), respectively. The substantially lower energy barrier calculated for the ethylene π-complex compared to the precatalyst (by ca. 3 kcal/mol) suggests that a rotation of the 2-phenylphenoxy ligand is even easier for the species involved in the polymerization cycle.

Full mechanistic DFT studies were carried out on representative examples of type 4 (**15**, **16**, and **18**), type 3 (**10** and **12**), and type 1 (**3**) complexes as well as the CGC as a reference. Figure 9 shows the energy profiles of the minimum-energy propagation pathways for compound **18** and CGC. In the first stage of the propagation mechanism, an alkyl β-agostic complex easily accommodates ethylene to form a π-complex, which is a direct starting point for the insertion reaction. There are three major types of ethylene π-complexes,[16] all corresponding to the minima on the potential energy surfaces. In particular, there are complexes with a straightened alkyl chain, i.e., without a β-agostic bond but with a weaker α-agostic interaction, (compounds **Ia**, **Ib**, and **III**), as well as two types of π-complexes, in which the alkyl remains in the β-agostic arrangement. Figure 9 gives two examples of one type of these β-agostic-π-complexes (compounds **IIa**, **IIb**, and **IV**). In these complexes (back-side π-complexes), ethylene is located on the side of the alkyl carbon atom. This gives rise to a back-side insertion pathway, which leads to the formation of a δ-agostic insertion product. In the last type of the π-complex (not shown), ethylene is located on the side of the β-agostic hydrogen (front-side π-complexes). Such complexes can lead directly to a chain termination reaction. A prior rotation of the alkyl group is essential for the insertion of ethylene via the front-side pathway to form compounds **Ia** or **Ib**. Therefore, compounds **Ia** and **Ib** are believed to be the direct starting points for the front-side insertion pathways. It is also important that there are several isomers for each type of π-complex. Figure 9a only shows the two minimum-energy insertion pathways for each front-side (starting from compounds **Ia** and **Ib**) and back-side (starting from compounds **IIa** and **IIb**) mechanism for compound **18**. The main difference in the geometry of the conformational isomers **Ia** and **Ib** (as well as in compounds **IIa** and **IIb**) lies in the position of a

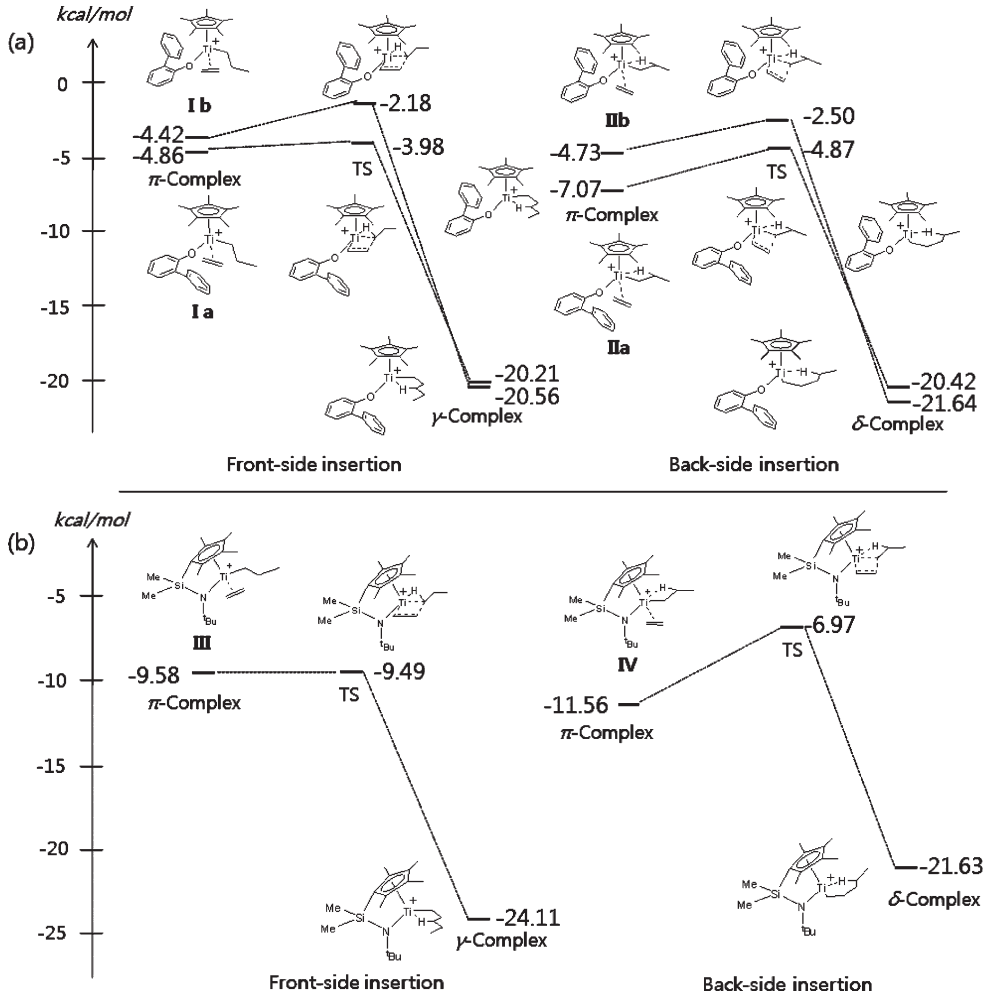

Figure 9. Energy profiles concerning possible ethylene π-complexes leading to the ethylene insertion of compound **18** and CGC: (a) ethylene insertion pathways starting from compound **18** and (b) ethylene insertion pathways starting from CGC.

phenyl substituent at the phenoxy ligand upon metal coordination. The conversion from **Ia** (and **IIa**) to energetically more favorable π-complexes **Ib** (and **IIb**) can be envisioned by revolving the phenylphenoxy ligand around the Ti−O−C(11) axis.

Figure 9b clearly shows that the activation energy of back-side insertion starting from the π-complex **IV** (4.59 kcal/mol) is substantially higher than the activation energy for the front-side insertion starting from the π-complex **III** (0.09 kcal/mol). The preference of the front-side insertion is also seen from the absolute energies of the two transition states: the front-side insertion TS is lower in energy by 2.52 kcal/mol (−9.49 vs −6.97 kcal/mol). This makes the back side insertion unlikely in the case of CGC.

In the case of **18** (Figure 9a) the activation energy for the front-side insertion starting from the π-complex **Ia** (0.88 kcal/mol) is also lower than the activation energy for the back-side insertion starting from the π-complex **IIa** (2.20 kcal/mol). However, the preferred back-side insertion TS has lower energy than the transition state for the front-side insertion by 0.89 kcal/mol (−4.87 vs −3.98 kcal/mol). This indicates that in the case of **18** both insertion mechanisms are viable, with a strong predominance of the back-side insertion.

Table 4 lists the calculated energies of the ethylene π-complexes and the corresponding transition states for all catalysts studied theoretically. The table includes only the minimum energy species of each type described above. These energy values were used to model the catalytic activity. The

Chart 3. (a) Contributions from the Front-Side and Back-Side Insertion to the Total Activity and (b) the Correlation between the Theoretical Activity Parameter, *v*, and the Experimental Data

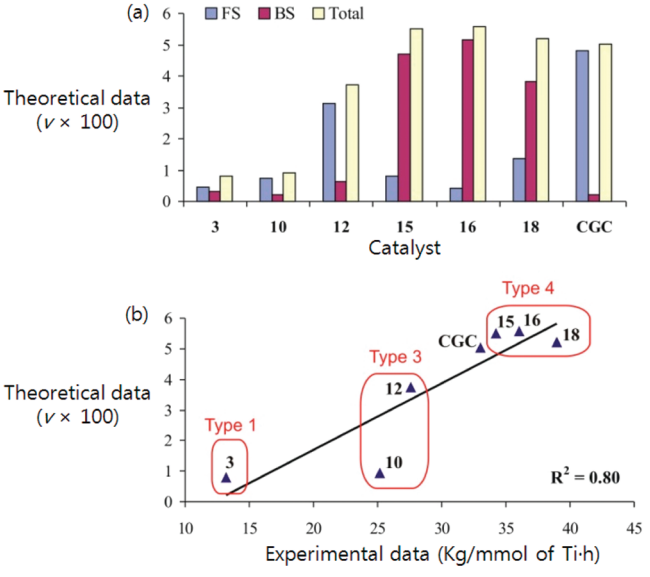

relative activity was estimated as a sum of the contributions from the possible insertion pathways to the overall propagation rate, $v = \Sigma_i k_i[\pi_i]$. In the above equation, k_i is the rate

Table 4. Relative Energies from the DFT Calculations with the ADF Program for One Complex of Type 1 (3), Two of Type 3 (10, 12), Three of Type 4 (15, 16, 18), and the Constrained Geometry Catalyst (CGC), as a Reference

catalyst	insertion/termination pathway	π-complex type	π-complex	transition state (TS)	γ-complex (δ-complex)
3	front-side	**I**	−10.43	−7.59	−24.74
	back-side	**II**	−10.46	−7.31	−23.95
	BHT	**BHT**	−11.18	−4.71	
10	front-side	**I**	−10.12	−7.44	−24.99
	back-side	**II**	−10.48	−6.39	−25.39
	BHT	**BHT**	−10.94	−4.91	
12	front-side	**I**	−8.14	−5.88	−24.46
	back-side	**II**	−5.98	−4.60	−24.63
	BHT	**BHT**	−8.12	−0.49	
15	front-side	**Ia**	−9.28	−6.85	−25.05
		Ib	−9.97	−7.64	−24.96
	back-side	**IIa**	−11.04	−9.35	−25.18
		IIb	−9.61	−5.32	−25.19
	BHT	**BHTa**	−10.21	−4.30	
		BHTb	−10.86	−4.25	
16	front-side	**Ia**	−9.07	−6.32	−24.44
		Ib	−9.47	−6.31	−24.13
	back-side	**IIa**	−10.49	−8.86	−24.59
		IIb	−9.20	−6.90	−24.94
	BHT	**BHTa**	−9.66	−3.77	
		BHTb	−10.38	−3.50	
18	front-side	**Ia**	−4.86	−3.98	−20.21
		Ib	−4.42	−2.18	−20.56
	back-side	**IIa**	−7.07	−4.87	−20.42
		IIb	−4.73	−2.50	−21.64
	BHT	**BHTa**	−6.67	−0.04	
		BHTb	−5.24	0.80	
CGC	front-side	**I**	−9.58	−9.49	−24.11
	back-side	**II**	−11.56	−6.97	−21.63
	BHT	**BHT**	−11.12	−3.16	

Table 5. Results of Co-Polymerization of Ethylene and 1-Octene at 140 °C[a]

									TOF ($\times 10^3$ min^{-1})[g]	
type	catalyst	yield (g)	activity[b]	MI[c] (g/10 min)	M_w[d] ($\times 10^4$)	M_w/M_n[d]	density[e] (g/mL)	1-octene[f] (mol %)	ethylene	1-octene
3	**11**	2.0	120	0.12	15.2	4.01	0.9058	3.71	61.8	2.4
	12	2.2	132	0.14	15.0	2.08	0.9139	2.99	69.8	2.2
	13	1.7	102	0.07	15.8	2.43	0.9115	3.10	53.8	1.7
	14	1.5	90	0.15	13.7	2.56	0.9162	2.32	48.8	1.2
4	**15**	4.6	276	0.16	13.0	3.34	0.9052	3.94	140.9	5.8
	16	5.2	312	0.18	11.5	2.15	0.9066	3.74	160.5	6.2
	17	3.8	228	0.19	10.7	4.15	0.9032	4.43	114.3	5.3
	18	5.9	354	0.02	16.4	3.01	0.9148	2.73	189.1	5.3
ref	**CGC**[h]	3.7	222	0.18	11.2	2.31	0.9154	2.55	119.4	3.1

[a] Polymerization conditions: semibatch type 200 mL autoclave reactor, cocatalyst = $[Ph_3C][B(C_6F_5)_4]$, scavenger = mMAO-7, solvent = cyclohexane, ethylene pressure = 30 kg/cm^2, total solution volume = 110 mL, catalyst = 1 μmol, [catalyst]:[cocatalyst]:[scavenger] = 1: 1.5: 100, comonomer = 1-octene(8 mL), reaction time = 1 min, and temperature = 140 °C. [b] Here, kg of polymer/(mmol of Ti·h). [c] Polymer melt index measured based on ASTM D2839 method. [d] Weight average molecular weight (g/mol) and molecular weight distribution were measured by PL210 GPC at 135 °C. [e] Polymer density measured by a density gradient column based on ASTM D 1505. [f] 1-Octene content (mol %) estimated by ^{13}C NMR spectra. [g] TOF was calculated from the ^{13}C NMR spectra. Turnover frequency = (molar amount of ethylene and/or 1-octene consumed)/(mol Ti·min). [h] $[Me_2Si(\eta^5\text{-}Me_4Cp)(N^tBu)]TiCl_2$.

constant for the i^{th} insertion pathway, which was estimated at a given temperature, T, from the insertion barrier. Likewise, $[\pi_i]$ is the concentration of the i^{th} π-complex, which was estimated from the Maxwell−Boltzmann distribution at T. It should be emphasized that in the approach applied here we take into account not only the rate constants (insertion barriers) but as well the statistical populations of crucial π-complexes at given temperature.

Chart 3 shows the contributions from the front- and back-side insertion to the total activity along with the correlation between the theoretical activity parameter, v, and experimental data. The results clearly show that the preference for back-side insertion is a unique feature of monosubstituted type 4 catalysts. For the CGC and disubstituted type 1 and type 3 complexes, the front-side insertion pathways make a dominating contribution to the catalyst activity, while the back-side insertion is almost negligible for those systems.

Furthermore, the theoretical activity parameter correlates very well with the experimental data, showing the highest values for the type 4 complexes. The preference for the back-side insertion mechanism for the type 4 systems, leading to increased activity, appears to be due to their conformational flexibility.

Ethylene and 1-Octene Copolymerization. The newly prepared complexes, types 3 and 4 and CGC, were tested for ethylene/1-octene copolymerization after activation with $Ph_3CB(C_6F_5)_4$ and mMAO-7. The mMAO-7 was added as both a scavenger and alkylating agent. Table 5 summarizes the polymerization conditions and results. Interestingly, compounds **15**−**18** [Type 4, 228−354 kg/(mmol of Ti·h)] showed much higher catalytic activity than those found in type 3 (**11**−**14**) [90−132 kg/(mmol of Ti·h)], and the activity of complex **18** reached 354 kg/(mmol of Ti·h). The dependence of the polymerization rate (turnover frequency, TOF)

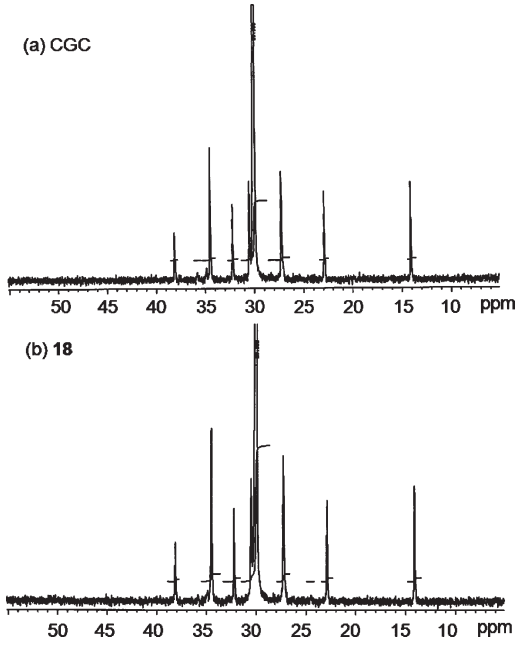

Figure 10. ^{13}C NMR spectra (10−50 ppm, in benzene-d_6 and 1,2,4-trichlorobenzene at 130 °C) for poly(ethylene-*co*-1-octene)s prepared by (a) CGC−$Ph_3CB(C_6F_5)_4$ (1-octene 2.55 mol %) and (b) **18**−$Ph_3CB(C_6F_5)_4$ (1-octene 2.73 mol %).

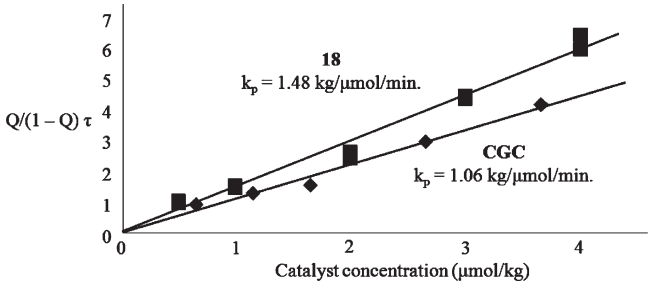

Figure 11. Kinetics of continuous ethylene and 1-octene copolymerization.

on the substituent followed a similar trend. The molecular weights of the polymers obtained by compound **18** (M_w= 164 000) are higher than those of the polymer obtained from compounds **15**−**17** (M_w= 107 000−130 000). The melt flow rate is dependent mainly on the molecular weight, and the molecular weight data obtained on the GPC were in agreement with the data of the melt index (MI) of the resins (0.16, 0.18, 0.19, and 0.02 g/10 min for compounds **15**, **16**, **17**, and **18**, respectively). Rather narrow molecular weight distributions (M_w/M_n= 2.15−4.15) were observed, indicating a single active species in the polymerization reaction. The activity and molecular weights (M_w) of the polymers obtained by compound **18** were higher than those of the polymer obtained with CGC [222 kg/(mmol of Ti·h) and M_w = 112 000, respectively]. The density of the resin was dependent mainly on the 1-octene content of the copolymer: the 1-octene content increased with decreasing density. A comparison of the densities of the polymers indicates that compound **18** (0.9148 g/mL) is slightly superior to CGC (0.9154 g/mL) in incorporating 1-octene, which was also confirmed by an analysis of the ^{13}C NMR spectra of the polymers (**18**, 2.73 mol % and CGC, 2.55 mol %).[17] (Figure 10) Interestingly, compound **18** showed better activity and 1-octene incorporation than CGC. Furthermore, the rate of incorporation and 1-octene content for compound **18** was higher than that of CGC when continuous reactor conditions were applied. (Figure 11 and SFigure 6, see Supporting Information)

Conclusion

Monosubstitution at the 2-position phenolate ligand is important for controlling the catalytic activity based on homopolymerization results. The phenylphenoxy ligand system (**18**) showed the best performance under high temperature polymerization conditions. The $^1H-^1H$ NOSEY data suggests a revolution of the phenoxy ligand and the $^1H-^1H$ ROSEY experiment indicated the stability of two possible conformer structures arising from the revolving phenoxide ligand. The DFT calculation agrees well with the NOSEY and ROESY data, which supports, a revolving ligand with a small rotational barrier of 4.3 kcal/mol for compound **18**. The DFT results clearly show that the preference for back-side insertion is a unique feature of monosubstituted type 4 catalysts, which is due to their conformational flexibility. The activity and comonomer content of the polymers obtained by compound **18** were higher than that of the polymer obtained by CGC.

Experimental Section

General Considerations. All manipulations were carried out under a dry nitrogen atmosphere using standard Schlenk techniques. Toluene, diethyl ether, hexane and cyclohexane were dried and distilled from sodium benzophenone. Acetonitrile was dried and distilled over P_2O_5. 1-Octene was purified using the Grubbs-type column systems. The ^1H and ^{13}C NMR spectra were recorded on a Varian Mercury 300 spectrometer operating at 300.1 and 75.44 MHz, respectively. The 2D $^1H-^1H$ NOESY NMR, 2D $^1H-^1H$ ROESY NMR, and variable-temperature ^1H NMR spectra were recorded on a Bruker AVANCE 800 spectrometer operating at 800.25 MHz (Korea Basic Science Institute), a Bruker AVANCE 500 spectrometer operating at 499.97 MHz, and a Bruker DRX 500 spectrometer operating at 500.13 MHz, respectively. ^{13}C NMR spectra for poly(ethylene-*co*-1-octene)s were recorded on a Bruker DRX 500 spectrometer (125.75 MHz) with proton decoupling. The copolymer samples for analysis were prepared by dissolving the polymers in 1,2,4-trichlorobenzene with 10 wt % benzene-d_6 solution, and the spectra were measured at 140 °C. All proton and carbon chemical shifts were measured relative to the internal residual toluene, benzene, chloroform and methylene chloride from the lock solvent (99.5% CD_5CD_3, 99.5% C_6D_6, 99.9% $CDCl_3$, and 99.9% CD_2Cl_2). Compounds **1**−**14** were obtained using previously reported procedures.[5c,9,11] All phenol reagents, palladium(II) acetate, boron tribromide (1.0 M in methylene chloride) and *n*-BuLi (2.5 M in hexane) were purchased from Aldrich Chemicals. Cp*$TiCl_3$, $Ph_3CB(C_6F_5)_4$, and mMAO-7 were purchased from Dalchem, Boulder Scientific, and Akzo Chemicals, respectively. All reagents were used without purification.

Crystal Structure Determination. Crystals of compounds **16**, **18**, and **21** were obtained from toluene at −15 °C, sealed in glass capillaries under argon and mounted on the diffractometer. A preliminary examination and data collection were carried out using a Bruker SMART CCD detector system, single-crystal X-ray diffractometer equipped with a sealed-tube X-ray source (40 kV × 50 mA) and graphite-monochromated Mo K_α radiation (λ = 0.71073 Å). The preliminary unit cell constants were determined using a set of 45 narrow-frame (0.3° in ω) scans. The double-pass method of scanning was used to exclude noise. The frames collected were integrated using an orientation matrix determined from the narrow-frame scans. The SMART software package was used for data collection, and SAINT was used for frame integration.[18a] The final cell constant was determined

by a global refinement of the xyz centroids of the reflections harvested from the entire data set. The structure solution and refinement were carried out using the SHELXTL-PLUS software package.[18b] Further detailed information is provided in Table 1.

Back Calculation of ROSEY Experiments. The structure determinations were carried out using HYGEOM, HYNMR. Sequential assignments of the amino acid spin systems were made using ROESY. Most importantly, the direct way for secondary structure determination was based on qualitative analysis of the ROESY spectrum.[19] The structures were calculated from the NMR data according to the standard HYGEOM simulated annealing and refinement protocols with minor modifications. The ROESY cross peaks were grouped into six categories according to their intensity. Most of the distance geometry (DG) algorithm accepts the input of the distance constraints from the ROESY measurements.[20] (1) A set of distance restraints or bounds obtained from the ROESY data were determined by the planarity restraints derived from the primary structure. This involves the selection of possible intervals between the lower and upper bounds. (2) Embedding. The values of the distances from within the bounds obtained by bound smoothing were estimated at random, and the atomic coordinates that represent the best-fit to this guess were generated. (3) Optimization. The deviations of the coordinates from the distance bounds, as well as the stereospecific assignments, were minimized. A 2D ROESY back calculation was performed when an additional conjugate gradient minimization (CGM) was unable to further reduce the penalty for a particular structure, and new distance restraints dictated by the discrepancies between the experimental and back-calculated spectra were added to the experimental restraint list. Freshly embedded DG structures minimized with the modified restraints list generally exhibited penalty values less than those of the previously refined structures, and the new DG structures generally gave back-calculated ROESY spectra that were more consistent with the experimental data.[21] The structure was calculated using the DG algorithm, HYGEOM. Ten separated structures were generated using all the constraints and random input. No further refinement by energy minimization was carried out on the output of the DG calculations. The rmsd (root-mean square distances) deviations between the NMR structures were 0.4 Å for the backbone.[20] The back-calculation was assigned to the GENNOE calculation in order to generate the theoretical ROESYs. Consecutive serial files, which were obtained from the GENNOE calculation, were incorporated into HYNMR to generate the ROESY back-calculation spectra, which can be compared directly with the experimental ROESY spectra.[22]

Computational Details. The DFT calculations based on the Becke−Perdew exchange-correlation functional[23] were carried out using the Amsterdam density functional (ADF) program, version 2004.01.[24] A standard double-ζ STO basis included in the ADF package with one set of polarization functions was applied to the H, C, N, O, Si, Cl atoms, while a standard triple-ζ basis set was employed for the Ti atom. The 1s electrons of C, N, O as well as the 1s−2p electrons of Ti, Si and Cl were treated as a frozen core. The auxiliary s, p, d, f, and g STO functions, which were centered on all nuclei, were used to fit the electron density and obtain accurate Coulomb and exchange potentials in each SCF cycle. Geometry optimization was performed for the titanium-based precatalyst, the cationic active species and intermediates in the catalytic cycle: β-agostic alkyl complexes and ethylene π-complexes, as well as the γ-agostic and δ-agostic insertion products. Transition state optimization was carried out for the insertion and termination TS, starting from the structures obtained from a series of constrained-optimizations with the particular C−C or C−H distance used as a respective reaction coordinate.

Ethylene Homopolymerization. Cyclohexane (105 mL) and mMAO-7 (0.1 mmol) were introduced to a thoroughly dried 200 mL autoclave reactor, which was heated to 140 °C. The reactor was pressurized to 30 kg/cm^2 with ethylene, and specific amounts of the catalyst and a $Ph_3CB(C_6F_5)_4$ toluene solution (5 mL) were added through a catalyst injector to initiate the polymerization reaction. During polymerization, the reactor pressure was maintained using a continuous ethylene feed. After 10 min, the reactor was cooled to 55 °C, degassed and 5 mL of acidic ethanol was added to quench the polymerization reaction. The solution was then poured into 1500 mL of ethanol, and the resulting polymer was recovered by filtration and dried in a vacuum at 70 °C for 12 h.

Ethylene and 1-Octene Copolymerization. Cyclohexane (97 mL), 1-octene (8 mL) and mMAO-7 (0.1 mmol) were introduced to a thoroughly dried 200 mL autoclave reactor, and the reactor was heated to 140 °C. The reactor was pressurized with ethylene up to 30 kg/cm^2, and specific amounts of the catalyst and $Ph_3CB(C_6F_5)_4$ toluene solution (5 mL) were then added through the catalyst injector to begin polymerization. During polymerization, the reactor pressure was maintained by continuously feeding ethylene. After 1 min, the reactor was cooled to 55 °C, degassed, and 5 mL of acidic ethanol was added to quench the polymerization reaction. The solution was then poured into 1500 mL of ethanol, and the resulting polymer was recovered by filtration and dried in a vacuum at 70 °C for 12 h.

Continuous Copolymerization of Ethylene and 1-Octene. A 400 mL CSTR (continuous stirred tank reactor) was used for copolymerization. The catalyst, cocatalyst, scavenger, cyclohexane, ethylene, and 1-octene were added continuously using metering pumps, and recovery of the unreacted monomer and solvent was also performed continuously. The CSTR was maintained at 150 °C and 110 kg/cm^2, and all process variables including the feed rates were computer-controlled using FIX software. Pelagonic acid was added to the product solution exiting the CSTR at a flow rate of 5.2 mmol/h to deactivate the catalyst residues. Subsequently, the unreacted monomers and solvent were removed from the polymer solution, and polymer product was recovered. Figure 11 shows $Q/(1-Q)\tau$ as a function of the catalyst concentration [μmolkg^{-1}], where Q and τ are the ethylene conversion and reactor hold-up time, respectively. The rate of ethylene disappearance is given by $-d[E]/dt = k_p[Cat^*][E]$, where [E] = ethylene concentration, [Cat*] = active catalyst concentration, and k_p = reaction rate constant. The CSTR system is given by $-d[E]/dt = V_{fl.}[E]_{in}Q/V_r$, where $V_{fl.}$ = volume of fluid, Q = ethylene conversion, $[E]_{in}$ = inlet ethylene concentration, $[E]_{out}$ = outlet ethylene concentration, V_r = volume of reactor. $k_p[Cat^*]V_{fl.}/V_r = Q/(1-Q)$ was derived by combining the two equations. $V_{fl.}/V_r$ is the reactor hold-up time (τ). Therefore, this equation becomes $k_p[Cat^*] = Q/[\tau(1-Q)]$. If $Q/[\tau(1-Q)]$ is plotted as a function of [Cat*], a straight line is obtained with a slope of k_p, as shown in Figure 11.

Preparation of 2-Bromo-6-methylphenol. Br_2 (0.77 mL, 15 mmol) was added dropwise to a solution of Me_2NH (2.09 mL, 16.5 mmol) and NaOH (1.32 g, 33 mmol) in 50 mL of H_2O at −15 °C. The mixture was stirred at this temperature for 30 min and extracted with toluene (100 mL). The organic layer was separated and dried with $MgSO_4$ to give a yellow solution of Me_2NBr, which was then added to a solution of *o*-cresol (1.30 g, 12 mmol) in 100 mL of toluene at −15 °C. The mixture was stirred for 4 h, warmed slowly to room temperature, stirred overnight, and then acidified with 20 mL of HCl (6 M). The organic layer was separated and dried with $MgSO_4$. The pure product was obtained as a colorless oil by column chromatography over silica (hexanes/CH_2Cl_2, 3:1). Yield: 1.57 g (70%). ^{1}H NMR ($CDCl_3$): δ 2.31 (s, 3H, CH_3), 5.57 (s, 1H, O*H*), 6.71 (t, 1H, *Ph*, $^3J_{H-H}$ = 7 Hz), 7.08 (d, 1H, *Ph*, $^3J_{H-H}$ = 7 Hz), 7.31 (d, 1H, *Ph*, $^3J_{H-H}$ = 7 Hz). ^{13}C NMR ($CDCl_3$): δ 16.73 (CH_3), 110.27 (Br-*C*), 121.33, 126.05, 129.47, 130.50, 150.50.

Preparation of 2-Bromo-6-isopropylphenol. A procedure analogous to the preparation of 2-bromo-6-methylphenol was employed but instead starting from 2-isopropylphenol (1.61 mL, 12 mmol). The pure product was obtained as a

colorless oil by column chromatography over silica (hexanes/CH_2Cl_2, 3:1). Yield: 1.93 g (75%). ^{1}H NMR ($CDCl_3$): δ 1.26 (d, 6H, CH(CH_3)$_2$, $^3J_{H-H}$ = 7 Hz), 3.35 (m, 1H, CH(CH$_3$)$_2$), 5.60 (s, 1H, OH), 6.79 (t, 1H, *Ph*, $^3J_{H-H}$ = 7 Hz), 7.15 (d, 1H, *Ph*, $^3J_{H-H}$ = 7 Hz), 7.32 (d, 1H, *Ph*, $^3J_{H-H}$ = 7 Hz). ^{13}C NMR ($CDCl_3$): δ 22.52 (CH(CH$_3$)$_2$), 28.16 (CH(CH$_3$)$_2$, 110.78 (Br−C), 121.60, 126.07, 129.21, 136.48, 149.54.

Preparation of 2-Bromo-6-*tert*-butylphenol. A procedure analogous to the preparation of 2-bromo-6-methylphenol was used but instead starting from 2-*tert*-butylphenol (1.84 mL, 12 mmol). The pure product was obtained as a colorless oil by column chromatography over silica (hexanes/ CH_2Cl_2, 3:1). Yield: 2.14 g (78%). ^{1}H NMR ($CDCl_3$): δ 1.41 (s, 9H, C(CH_3)$_3$), 5.80 (s, 1H, OH), 6.74 (t, 1H, *Ph*, $^3J_{H-H}$ = 7 Hz), 7.24 (d, 1H, *Ph*, $^3J_{H-H}$ = 7 Hz), 7.35 (d, 1H, *Ph*, $^3J_{H-H}$ = 7 Hz). ^{13}C NMR ($CDCl_3$): δ 29.48 (C(CH$_3$)$_3$), 35.49 (C(CH$_3$)$_3$), 112.41 (Br−C), 121.09, 126.65, 129.76, 137.88, 150.56.

Preparation of 2-Bromo-6-methylanisole. A mixture of 2-bromo-6-methylphenol (1.87 g, 10 mmol), K_2CO_3 (4.15 g, 30 mmol), and iodomethane (0.75 mL, 12 mmol) was dissolved in CH_3CN (40 mL) and heated under reflux for 4 h in nitrogen. The reaction mixture was allowed to cool to room temperature, extracted with diethyl ether (3 × 30 mL) and dried over $MgSO_4$. The volatile solvent was removed under reduced pressure, and the pure product was obtained as a colorless oil by column chromatography over silica (hexanes/EA, 100:1). Yield: 1.91 g (95%). ^{1}H NMR ($CDCl_3$): δ 2.33 (s, 3H, CH_3), 3.81 (s, 3H, OCH_3), 6.87 (t, 1H, *Ph*, $^3J_{H-H}$ = 7 Hz), 7.10 (d, 1H, *Ph*, $^3J_{H-H}$ = 7 Hz), 7.33 (d, 1H, *Ph*, $^3J_{H-H}$ = 7 Hz). ^{13}C NMR ($CDCl_3$): δ 17.13 (CH$_3$), 55.90 (OCH$_3$), 111.50, 126.98, 129.65, 131.76, 151.72 (C_{ipso}).

Preparation of 2-Bromo-6-isopropylanisole. A procedure analogous to the preparation of 2-bromo-6-methylanisole was employed but instead starting from 2-bromo-6-isopropylphenol (2.15 g, 10 mmol). The pure product was obtained as a colorless oil by column chromatography over silica (hexanes/EA, 100:1). Yield: 2.11 g (92%). ^{1}H NMR ($CDCl_3$): δ 1.27 (d, 6H, CH-(CH_3)$_2$), 2.93 (m, 1H, CH(CH$_3$)$_2$), 3.80 (s, 3H, OCH_3), 6.92 (t, 1H, *Ph*, $^3J_{H-H}$ = 7 Hz), 7.20 (d, 1H, *Ph*, $^3J_{H-H}$ = 7 Hz), 7.36 (d, 1H, *Ph*, $^3J_{H-H}$ = 7 Hz). ^{13}C NMR ($CDCl_3$): δ 24.36 (CH-(CH$_3$)$_2$), 33.49 (CH(CH$_3$)$_2$, 55.83 (OCH$_3$), 111.34, 126.32, 129.69, 139.02, 154.71 (C_{ipso}).

Preparation of 2-Bromo-6-*tert*-butylanisole. A procedure analogous to the preparation of 2-bromo-6-methylanisole was used but instead starting from 2-bromo-6-*tert*-butylphenol (2.29 g, 10 mmol). The pure product was obtained as a colorless oil by column chromatography over silica (hexanes/EA, 100:1). Yield: 2.19 g (90%). ^{1}H NMR ($CDCl_3$): δ 1.44 (s, 9H, C(CH_3)$_3$), 3.28 (s, 3H, OCH_3), 7.08 (t, 1H, *Ph*, $^3J_{H-H}$ = 7 Hz), 7.17 (d, 1H, *Ph*, $^3J_{H-H}$ = 7 Hz), 7.36 (d, 1H, *Ph*, $^3J_{H-H}$ = 7 Hz). ^{13}C NMR ($CDCl_3$): δ 30.98 (C(CH$_3$)$_3$), 35.31 (C(CH$_3$)$_3$), 55.79 (OCH$_3$), 123.29, 126.30, 129.92, 140.13, 157.64 (C_{ipso}).

Preparation of 2-Methyl-6-phenylphenol. 2-Bromo-6-methylanisole (1.41 g, 7 mmol), phenylboronic acid (0.94 g, 7.7 mmol), K_3PO_4 (4.90 g, 23.1 mmol), palladium(II) acetate (0.08 g, 5 mol %), and tris(2-methoxyphenyl)phosphine (0.37 g, 15 mol %) were added to a two-phase mixture of dimethoxyethane (40 mL) and water (10 mL). The resulting mixture was stirred under nitrogen at 80 °C for 12 h. The reaction mixture was cooled to room temperature, extracted with diethyl ether (3 × 30 mL) and dried over magnesium sulfate. The solvent was removed under reduced pressure, and the residue was purified by silica gel column chromatography using hexane/EA (5:1) as an eluent. 2-Methyl-6-phenylanisole was obtained as a colorless oil (1.28 g, 92%). BBr_3 (7.2 mL, 7.2 mmol) was then added through syringe to a solution of 2-methyl-6-phenylanisole (1.28 g, 6.5 mmol) in CH_2Cl_2 at −78 °C. The mixture was warmed slowly to room temperature, stirred overnight, and the organic layer was separated with diethyl ether (3 × 30 mL) and dried with $MgSO_4$. The pure product was obtained as a white powder by column chromatography over silica (hexanes/CH_2Cl_2, 1.5:1). Yield: 1.09 g (91%). ^{1}H NMR ($CDCl_3$): δ 2.33 (s, 3H, CH_3), 5.27 (s, 1H, OH), 6.91 (t, 1H, *Ph*, $^3J_{H-H}$ = 7 Hz), 7.10 (d, 1H, *Ph*, $^3J_{H-H}$ = 7 Hz), 7.17 (d, 1H, *Ph*, $^3J_{H-H}$ = 7 Hz), 7.46 (m, 5H, *Ph*). ^{13}C NMR ($CDCl_3$): δ 16.32 (CH$_3$), 120.35, 124.78, 127.79, 127.87 127.99 128.82, 129.29, 129.48, 130.63, 137.49, 150.71 (C_{ipso}).

Preparation of 2-Isopropyl-6-phenylphenol. A procedure analogous to the preparation of 2-methyl-6-phenylphenol was used but instead starting from 2-bromo-6-isopropylanisole (1.60 g, 7 mmol). The pure product was obtained as a white powder by column chromatography over silica (hexanes/CH_2Cl_2, 1.5:1). Overall yield: 1.23 g (83%). ^{1}H NMR ($CDCl_3$): δ 1.32 (d, 6H, CH(CH_3)$_2$, $^3J_{H-H}$ = 7 Hz), 3.14 (m, 1H, CH(CH$_3$)$_2$), 5.37 (s, 1H, OH), 6.94 (t, 1H, *Ph*, $^3J_{H-H}$ = 7 Hz), 7.12 (d, 1H, *Ph*, $^3J_{H-H}$ = 7 Hz), 7.27 (d, 1H, *Ph*, $^3J_{H-H}$ = 7 Hz), 7.49 (m, 5H, *Ph*). ^{13}C NMR ($CDCl_3$): δ 23.52 (CH(CH$_3$)$_2$), 33.20 (CH(CH$_3$)$_2$, 120.13, 126.97, 128.09, 129.24, 129.69, 137.43, 150.97 (C_{ipso}).

Preparation of 2-*tert*-Butyl-6-phenylphenol. A procedure analogous to the preparation of 2-methyl-6-phenylphenol was employed but instead starting from 2-bromo-6-*tert*-butylanisole (1.70 g, 7 mmol). The pure product was obtained as a white powder by column chromatography over silica (hexanes/CH_2Cl_2, 1.5:1). Overall yield: 1.25 g (79%). ^{1}H NMR ($CDCl_3$): δ 1.53 (s, 9H, C(CH_3)$_3$), 5.52 (s, 1H, OH), 6.99 (t, 1H, *Ph*, $^3J_{H-H}$ = 7 Hz), 7.15 (d, 1H, *Ph*, $^3J_{H-H}$ = 7 Hz), 7.40 (d, 1H, *Ph*, $^3J_{H-H}$ = 7 Hz), 7.53 (m, 5H, *Ph*). ^{13}C NMR ($CDCl_3$): δ 29.78 (C(CH$_3$)$_3$), 35.08 (C(CH$_3$)$_3$), 120.03, 126.75, 128.12, 128.94, 129.59, 129.70, 136.37, 137.42, 151.15 (C_{ipso}).

Synthesis of Cp*Ti(O-2-MeC$_6$H$_4$)Cl$_2$ (15). A solution of Li-(O-2-MeC$_6$H$_4$) in toluene [prepared in situ by a reaction of *n*-BuLi (2.2 mL of a commercial 2.5 M solution in hexane, 5.55 mmol) and *o*-cresol (0.55 g, 5.05 mmol)] was added through a cannula to a solution of Cp*$TiCl_3$ (1.46 g, 5.05 mmol) in toluene at −78 °C. The mixture was warmed to room temperature and stirred for 12 h. The mixture was filtered through a Celite pad and the toluene was removed in a vacuum, leaving a red solid. Recrystallization from toluene at −15 °C produced compound **15** as red crystals. Yield: 1.55 g (85%). ^{1}H NMR (C_6D_6): δ 1.89 (s, 15H, C$_5$(CH_3)$_5$), 2.20 (s, 3H, CH_3), 6.80 (m, 1H, *Ph*), 6.94 (m, 3H, *Ph*). ^{13}C NMR (C_6D_6): δ 12.77 (C$_5$(CH$_3$)$_5$), 16.93 (CH$_3$), 120.59, 123.37, 127.16, 131.06 (C_5(CH$_3$)$_5$), 132.28, 134.02, 163.92 (C_{ipso}).

Synthesis of Cp*Ti(O-2-^{i}PrC$_6$H$_4$)Cl$_2$ (16). A procedure analogous to the synthesis of compound **15** was used but instead starting from 2-isopropylphenol (0.68 mL, 5.05 mmol). Recrystallization from toluene at −15 °C produced compound **16** as red crystals. Yield: 1.57 g (80%). ^{1}H NMR (C_6D_6): δ 1.18 (d, 6H, CH(CH_3)$_2$, $^3J_{H-H}$ = 7 Hz), 1.87 (s, 15H, C$_5$(CH_3)$_5$), 3.41 (m, 1H, CH(CH$_3$)$_2$), 6.87 (m, 1H, *Ph*), 6.93 (s, 2H, *Ph*), 7.08 (d, 1H, *Ph*, $^3J_{H-H}$ = 7 Hz). ^{13}C NMR (C_6D_6): δ 13.68 (C$_5$(CH$_3$)$_5$), 23.65 (CH(CH$_3$)$_2$), 27.54 (CH(CH$_3$)$_2$), 121.41, 124.16, 126.72, 127.28, 132.60, 139.21, 163.03 (C_{ipso}).

Synthesis of Cp*Ti(O-2-^{t}BuC$_6$H$_4$)Cl$_2$ (17). A procedure analogous to the synthesis of compound **15** was used but instead starting from 2-*tert*-butylphenol (0.78 mL, 5.05 mmol). Recrystallization from toluene at −15 °C produced compound **17** as red crystals. Yield: 1.53 g (75%). ^{1}H NMR (C_6D_6): δ 1.44 (s, 9H, C(CH_3)$_3$), 1.93 (s, 15H, C$_5$(CH_3)$_5$), 6.91 (m, 1H, *Ph*), 7.02 (s, 2H, *Ph*), 7.24 (d, 1H, *Ph*, $^3J_{H-H}$ = 7 Hz). ^{13}C NMR (C_6D_6): δ 12.98 (C$_5$(CH$_3$)$_5$), 30.17 (C(CH$_3$)$_3$), 35.12 (C(CH$_3$)$_3$), 123.62, 124.33, 127.05, 127.52, 132.54, 138.88, 163.87 (C_{ipso}).

Synthesis of Cp*Ti(O-2-PhC$_6$H$_4$)Cl$_2$ (18). A procedure analogous to the synthesis of compound **15** was employed but instead starting from 2-phenylphenol (0.86 g, 5.05 mmol). Recrystallization from toluene at −15 °C produced compound **18** as red crystals. Yield: 1.82 g (85%). ^{1}H NMR (C_6D_6): δ 1.67 (s, 15H, C$_5$*Me*$_5$), 6.82 (t, 1H, *Ph*, $^3J_{H-H}$ = 7 Hz), 6.95 (t, 1H, *Ph*, $^3J_{H-H}$ = 7 Hz), 7.05 (t, 1H, *Ph*, $^3J_{H-H}$ = 7 Hz), 7.17 (m, 2H, *Ph*), 7.23 (t, 2H, *Ph*, $^3J_{H-H}$ = 7 Hz), 7.55 (d, 2H, *Ph*,

$^3J_{H-H}$ = 7 Hz). ^{13}C NMR (C_6D_6): δ 12.27 ($C_5(CH_3)_5$), 121.52, 123.53, 127.10, 128.16, 128.50, 128.84, 130.34 ($C_5(CH_3)_5$), 132.32, 138.03, 162.00 (C_{ipso}).

Synthesis of Cp*Ti(O-2-Me-6-Ph−C_6H_4)Cl_2 (19). A procedure analogous to the synthesis of compound **15** was utilized but starting from 2-methyl-6-phenylphenol (0.93 g, 5.05 mmol). Recrystallization from toluene at −15 °C produced compound **19** as red crystals. Yield: 1.83 g (83%). ^{1}H NMR (C_6D_6): δ 1.62 (s, 15H, C_5Me_5), 2.40 (s, 3H, CH_3), 6.87 (t, 1H, *Ph*, $^3J_{H-H}$ = 7 Hz), 7.12 (m, 3H, *Ph*), 7.29 (t, 2H, *Ph*, $^3J_{H-H}$ = 7 Hz), 7.65 (d, 2H, *Ph*, $^3J_{H-H}$ = 7 Hz). ^{13}C NMR (C_6D_6): δ 12.43 ($C_5(CH_3)_5$), 18.85 (CH_3), 123.50, 127.27, 128.84, 129.14, 130.48, 131.09, 132.37, 154.32 (C_{ipso}).

Synthesis of Cp*Ti(O-2-^{i}Pr-6-Ph−C_6H_4)Cl_2 (20). A procedure analogous to the synthesis of compound **15** was used but instead starting from 2-isopropyl-6-phenylphenol (1.07 g, 5.05 mmol). Recrystallization from toluene at −15 °C produced compound **20** as red crystals. Yield: 1.88 g (80%). ^{1}H NMR (C_6D_6): δ 1.33 (d, 6H, $CH(CH_3)_2$, $^3J_{H-H}$ = 7 Hz), 1.63 (s, 15H, $C_5(CH_3)_5$), 3.53 (m, 1H, $CH(CH_3)_2$), 6.95 (t, 1H, *Ph*, $^3J_{H-H}$ = 7 Hz), 7.13 (m, 3H, *Ph*), 7.30 (t, 2H, *Ph*, $^3J_{H-H}$ = 7 Hz), 7.67 (d, 2H, *Ph*, $^3J_{H-H}$ = 7 Hz). ^{13}C NMR (C_6D_6): δ 12.42 ($C_5(CH_3)_5$), 24.24 ($CH(CH_3)_2$), 26.93 ($CH(CH_3)_2$), 123.90, 125.66, 127.24, 128.84, 128.98, 129.33, 131.28, 132.30, 133.52, 138.85, 140.91, 159.21 (C_{ipso}).

Synthesis of Cp*Ti(O-2-^{t}Bu-6-Ph−C_6H_4)Cl_2 (21). A procedure analogous to the synthesis of compound **15** was used but instead starting from 2-*tert*-butyl-6-phenylphenol (1.14 g, 5.05 mmol). Recrystallization from toluene at −15 °C produced compound **21** as red crystals. Yield: 1.89 g (78%). ^{1}H NMR (C_6D_6): δ 1.53 (s, 9H, $C(CH_3)_3$), 1.63 (s, 15H, $C_5(CH_3)_5$), 6.89 (t, 1H, *Ph*, $^3J_{H-H}$ = 7 Hz), 7.13 (m, 2H, *Ph*), 7.28 (t, 3H, *Ph*, $^3J_{H-H}$ = 7 Hz), 7.71 (d, 2H, *Ph*, $^3J_{H-H}$ = 7 Hz). ^{13}C NMR (C_6D_6): δ 12.69 ($C_5(CH_3)_5$), 31.21, 35.79, 123.30, 126.49, 127.27, 128.97, 131.19, 131.99, 133.10, 136.09, 139.54, 140.89, 162.67 (C_{ipso}).

Acknowledgment. We thank the Korea Basic Science Institute (KBSI) for running NMR experiments (Bruker AVANCE 800 spectrometer). This research was supported by MKE (The Ministry of Knowledge Economy), Korea, under the ITRC support program supervised by the IITA (Institute for Information Technology Advancement)" (IITA-2009-C1090-0902-0025) and a research grant from the Ministry of Science and Higher Education in Poland (2275-B-H03-2008-34).

Supporting Information Available: A file containing a table with the results from ethylene homopolymerization and figures showing the NOESY and ROESY NMR spectrum, ^{13}C NMR spectra of ethylene and 1-octene copolymer (with text explaning the results), and polymer density of continuous reactor, a file contining a table of structure and energetics of the full account of investigated species, and a .zip file containing three .cif files for **16**, **18**, and **21**, respectively. This material is available free of charge via the Internet at http://pubs.acs.org.

References and Notes

(1) (a) Biritovsek, G. J. P.; Gibson, V. C.; Wass, D. F. *Angew. Chem., Int. Ed. Engl.* **1999**, *38*, 428. (b) Gibson, V. C.; Spitzmesser, S. K. *Chem. Rev.* **2003**, *103*, 283.
(2) Kakugo, M. *Macromol. Symp.* **2001**, *174*, 295.
(3) Halle, R. W.; Malakoff, A. M. *J. Plast. Film Sheeting* **2005**, *21*, 13.
(4) Chum, S. P.; Kao, C. I.; Knight, G. W. In *Metallocene-based Polyolefins: Preparation, properties and technology*, Scheirs, J., Kaminsky, W., Eds.; Wiley Series in Polymer Science; John Wiley & Sons; Chichester, U.K., 2000; pp 161−286.
(5) (a) Sita, L. R.; Babcock, R. *Organometallics* **1998**, *17*, 5228. (b) Zhang, S.; Piers, W. E.; Gao, X.; Parvez, M. *J. Am. Chem. Soc.* **2000**, *122*, 5499. (c) Manz, T. A.; Phomphrai, K.; Medvedev, G.; Krishnamurthy, B. B.; Sharma, S.; Hag, J.; Novstrup, K. A.; Thomson, K. T.; Delgass, W. N.; Caruthers, J. M.; Abu-Omar, M. M. *J. Am. Chem. Soc.* **2007**, *129*, 3776.
(6) (a) Chen, Y. −X.; Marks, T. J. *Organometallics* **1997**, *16*, 3649. (b) Stevens, J. C. *Stud. Surf. Sci. Catal.* **1994**, *89*, 277. (c) Stevens, J. C. *Stud. Surf. Sci. Catal.* **1996**, *101*, 11. (d) Stevens, J. C.; Timmers, F. J.; Wilson, D. R.; Schmidt, G. F.; Nickias, P. N.; Rosen, R. K.; Knight, G. W.; Lai, S. Y. *EP 90−309496 416815, 19900830*, **1991**.
(7) (a) Hanaoka, H.; Hino, T.; Nabika, M.; Kohno, T.; Yanagi, K.; Oda, Y.; Imai, A.; Mashima, K. *J. Organomet. Chem.* **2007**, *692*, 4717. (b) Katayama, H.; Nabika, M.; Imai, A.; Miyashita, A.; Watanabe, T.; Johohji, H.; Oda, Y.; Hanaoka, H. *PCT Appl. WO 97−03992*, **1997**.
(8) (a) Stephan, D. W.; Stewart, J. C.; Guerin, F.; Courtenay, S.; Kickham, J.; Hollink, E.; Beddie, C.; Hoskin, A.; Graham, T.; Wei, P.; Spence, R. E. v. H.; Xu, W.; Koch, L.; Gao, X.; Harrison, D. G. *Organometallics* **2003**, *22*, 1937. (b) Stephan, D. W.; Stewart, J. C.; Guerin, F.; Spence, R. E. v. H.; Xu, W.; Harrison, D. G. *Organometallics* **1999**, *18*, 1116.
(9) (a) Nomura, K.; Naga, N.; Miki, M.; Yanagi, K.; Imai, A. *Organometallics* **1998**, *17*, 2152. (b) Nomura, K.; Naga, N.; Miki, M.; Yanagi, K. *Macromolecules* **1998**, *31*, 7588.
(10) Phomphrai, K.; Fenwick, A. E.; Sharma, S.; Fanwick, P. E.; Caruthers, J. M.; Delgass, W. N.; Abu-Omar, M. M.; Rothwell, I. P. *Organometallics* **2006**, *25*, 214.
(11) (a) Sturla, S. J.; Buchwald, S. L. *Organometallics* **2002**, *21*, 739. (b) Nomura, K.; Tanaka, A.; Katao, S. *J. Mol. Catal. A* **2006**, *254*, 197.
(12) (a) Suezawa, H.; Yoshida, T.; Umezawa, Y.; Tsuboyama, S.; Nishio, M. *Eur. J. Inorg. Chem.* **2002**, 3148. (b) Scrivanti, A.; Benetollo, F.; Venzo, A.; Bertoldini, M.; Beghetto, V.; Matteoli, U. *J. Organomet. Chem.* **2007**, *692*, 3577.
(13) Nielson, A. J.; Harrison, J. A.; Shen, C.; Waters, J. M. *Polyhedron* **2006**, *25*, 1729.
(14) (a) Velders, A. H.; Hotze, A. C. G.; Albada, G. A. v.; Haasnoot, J. G.; Reedijk, J. *Inorg. Chem.* **2000**, *39*, 4073. (b) Montoya, V.; Pons, J.; Solans, X.; Font-bardia, M.; Ros, J. *Inorg. Chim. Acta* **2005**, *358*, 2312. (c) Ghesner, I.; Fenwick, A.; Stephan, D. W. *Organometallics* **2006**, *25*, 4985.
(15) (a) Summers, M. F.; South, T. L.; Kim, B.; Hare, D. R. *Biochemistry* 1990, *29*, 329. (b) Blake, P.; Hare, D. R.; Summers, M. F. *Techniques in Protein Chemistry*; Villefranca, J. J., Ed.; Academic Press: New York, 1991; p 357. (c) South, T.; Blake, P.; Hare, D.; Summers, M. F. *Biochemistry* 1991, *30*, 6342.
(16) (a) Lohrenz, J. C. W.; Woo, T. K.; Fan, L.; Ziegler, T. *J. Organomet. Chem.* **1995**, *497*, 91. (b) Lohrenz, J. C. W.; Woo, T. K.; Ziegler, T. *J. Am. Chem. Soc.* **1995**, *117*, 12793. (c) Margl, P.; Deng, L.; Ziegler, T. *Organometallics* **1998**, *17*, 933. (d) Margl, P.; Deng, L.; Ziegler, T. *J. Am. Chem. Soc.* **1998**, *120*, 5517.
(17) Randall, J. *J. Macromol. Sci., Rev. Macro. Chem. Phys.* **1989**, *C29*, 201.
(18) (a) *SMART and SAINT*; Brucker Analytical X-ray Division, Madison, WI, 2002. (b) Sheldrick, G. M. *SHELXTL-PLUS Software Package*; Brucker Analytical X-ray Division, Madison, WI, 2002.
(19) Wuthrich, K. *NMR of Proteins and Nucleic Acids*; Wiley: New York, 1986.
(20) Evans, J. N. S. *Biomolecular NMR Spectroscopy*; Oxford Univ. Press: Oxford, U.K., 1995.
(21) South, T. L.; Blake, P. R.; Hare, D. R.; Summers, M. F. *Biochemistry* **1991**, *30*, 6342.
(22) Kim, D.; Rho, J.; Won, H. *J. Kor. Magn. Res. Soc.* **1999**, *3*, 44.
(23) (a) Becke, A. *Phys. Rev. A* **1988**, *38*, 3098. (b) Perdew, J. P. *Phys. Rev. B* **1986**, *34*, 7406. (c) Perdew, J. P. *Phys. Rev. B* **1986**, *33*, 8822.
(24) (a) TeVelde, G; Bickelhaupt, F. M.; Baerends, E. J.; Fonseca Guerra, C.; Van Gisbergen, S. J. A.; Snijders, J. G.; Ziegler, T. *J. Comput. Chem.* **2001**, *22*, 931 and references therein. . (b) Baerends, E. J.; Ellis, D. E.; Ros, P. *Chem. Phys.* **1973**, *2*, 41. (c) Baerends, E. J.; Ros, P. *Chem. Phys.* **1973**, *2*, 52. (d) te Velde, G.; Baerends, E. J. *J. Comput. Phys.* **1992**, *99*, 84. (e) Fonseca, C. G.; Visser, O.; Snijders, J. G.; te Velde, G.; Baerends, E. J. In *Methods and Techniques in Computational Chemistry*, METECC-95; Clementi, E., Corongiu, G., Eds.; STEF: Cagliari, Italy, 1995; p 305.